

Defect-mediated phase transition temperature of VO₂ (M) nanoparticles with excellent thermochromic performance and low threshold voltage†

Cite this: *J. Mater. Chem. A*, 2014, 2, 4520

Received 21st November 2013
Accepted 8th January 2014

DOI: 10.1039/c3ta14822j

www.rsc.org/MaterialsA

Ming Li,^{‡a} Xing Wu,^{‡c} Liang Li,^a Yuxi Wang,^c Dengbing Li,^a Jing Pan,^a Sijia Li,^c Litao Sun^{*c} and Guanghai Li^{‡*ab}

This paper reports the phase transition temperature regulation of VO₂ (M) nanoparticles using interfacial defects and size effect other than the traditional doping routine. The nanoparticles exhibit excellent thermochromic performance and a low threshold voltage.

Monoclinic vanadium dioxide [VO₂ (M)] has long been regarded as an attractive thermochromic material for energy-saving applications.^{1–3} However, it has been not immediately applicable for use as an intelligent window coating since it was reported in the early 1980s.⁴ A low luminous transmittance, unfavourable solar energy management and a relatively high phase transition temperature are three particularly challenging problems.⁵ The T_c can generally be reduced by doping VO₂ (M) with ions such as W⁶⁺, Mo⁶⁺, Ta⁵⁺, Nb⁵⁺ and Ru⁴⁺,⁶ but this is always accompanied by the degradation of its optical properties.⁷ Recent reports have found that oxygen vacancies can be used to tune the T_c over a wide range.⁸ This study aims to refine the T_c of VO₂ (M) using defect engineering. Indeed, both the T_c and the width and shape of the phase transition hysteresis strongly depend on the internal structure of VO₂ (M), and are characterized by a small lattice distortion, resulting in the pairing of vanadium atoms and a distinct band structure. Thus, the phase transition characteristics are critically influenced by the crystallinity and particle size/microstructure of VO₂ (M).⁵

Theoretical calculations have indicated that VO₂ (M) nanoparticles (NPs) with sizes much smaller than wavelength used can provide superior luminous transmittance and solar energy transmittance modulation.⁹ Unfortunately, the commercially

available forms of VO₂ are limited to bulk powders of large primary particle sizes,¹⁰ which greatly hinders its practical application in industry.

In this paper, we report a simple strategy for the synthesis of VO₂ (M) NPs, which is low-cost and large scale, by combining hydrothermal synthesis with a subsequent mild thermal treatment.

Various phase transition behaviors with different phase transition temperatures have been observed for the VO₂ (M) NPs, depending strongly on the post annealing conditions that control the grain size and interfacial defects. The VO₂ (M) NPs exhibited an excellent thermochromic performance with high visible-light transmittance and a large near infrared light modification ability. Meanwhile, it was found that the phase transition of the VO₂ (M) NPs can be triggered using an external electric field with a voltage of about 1 V at room temperature.

The VO₂ (M) NPs were prepared using a hydrothermal method and subsequent mild annealing treatment. The starting materials were a mixture of vanadium pentoxide (0.73 M), oxalic acid dehydrate (molar ratio: 1 : 1–2), polyvinylalcohol (1–2 wt%) and propylene glycol methyl ether acetate (1–2 wt%). The hydrothermal synthesis was performed in a 50 L autoclave (or in an autoclave with a smaller volume, such as 200 mL) with filling ratio of 60% at 220 °C over 36 h. After cooling down to room temperature, the resulting nanopowders were collected by centrifugation, washed alternately with copious amounts of deionized water and ethanol in order to remove any organic residue, and then dried in air at 70 °C. In order to obtain VO₂ (M), the as-prepared nanopowders were annealed in a vacuum furnace at 300–450 °C for different times.

The morphology and phase structure of the nanopowders were examined using field-emission scanning electron microscopy (FESEM, Sirion 200) and X-ray diffraction with the Cu K α_1 line (XRD, Philips X'Pert). High resolution TEM analysis was carried out using an image aberration corrected TEM (FEI Titan 80-300). A low accelerating voltage of 80 kV was used in order to avoid beam irradiation induced damage. Differential scanning calorimetry (DSC) analysis was performed using a Dupont

^aKey Laboratory of Materials Physics, Anhui Key Laboratory of Nanomaterials and Nanotechnology, Institute of Solid State Physics, Chinese Academy of Sciences, Hefei 230031, P. R. China. E-mail: ghli@issp.ac.cn

^bUniversity of Science and Technology of China, Hefei 230026, P. R. China

^cSEU-FEI Nano-Pico Center Key Laboratory of MEMS of Ministry of Education Southeast University, Nanjing, P. R. China. E-mail: slt@seu.edu.cn

† Electronic supplementary information (ESI) available: Experimental details and supporting results. See DOI: 10.1039/c3ta14822j

‡ These authors contributed equally to this work.

differential thermal analyzer under a flow of nitrogen at a heating rate of $10\text{ }^{\circ}\text{C min}^{-1}$. Optical transmission spectra were recorded using a UV-3600 spectrophotometer (Shimadzu ISR-260) equipped with a heating device. A nanofactory instruments STM-TEM holder was used for *in situ* manipulation and the electrical measurements. The holder contains both a fixed and movable contact terminal. A gold wire attached to a copper grid (2000 mesh) by conductive epoxy was loaded into the fixed terminal. In addition, a tungsten nanotip etched using an electrochemical method^{11,12} was added to the movable contacting terminal. The as-prepared VO₂ NPs dispersed in ethanol solution were dropped onto the copper grid. After assembling the set-up in the STM-TEM holder, a voltage can be applied to the fixed contact terminal while the movable terminal is grounded. The film thickness was measured by surface profilometry and metrology (Ambios XP-1) using a diamond needle.

Fig. 1a and b show FESEM images of the as-prepared VO₂ NPs. One can see that the NPs are uniformly distributed, have an average size of about 70 nm (see inset in Fig. 1a) and are produced on a large scale (see the photograph in the inset of Fig. 1b, which shows about 3 kg per 50 L pot). The VO₂ prepared directly from the hydrothermal treatment in the present study can be assigned to the recently reported new phase, VO₂ (D) (Fig. S1†).^{13,14} It is worth noting that VO₂ has many polymorphic forms, such as VO₂ (A), VO₂ (B) and VO₂ (C), and the VO₂ was designated as VO₂ (D) according to the literature. Due to the high resemblance, a mild thermal treatment condition would be sufficient to trigger a phase transition from VO₂ (D) to the high temperature rutile VO₂ (R) phase.¹³ There is no obvious change in the size and dispersity of the VO₂ (M) NPs after the annealing treatment, as seen from the TEM image in Fig. 1c and the size distribution histograms (Fig. S2†). The selected area electron diffraction (SAED) pattern in Fig. 1c can be indexed as the (100) and (011) reflections according to the monoclinic phase of the VO₂ NPs. Fig. 1d shows XRD patterns of

the VO₂ (M) NPs after annealing VO₂ (D) in a vacuum environment ($\sim 20\text{ Pa}$) at different temperatures for 1 h. It can be seen from the patterns that VO₂ (D) has completely transformed to VO₂ (M) even at a temperature of 300 °C. From this figure, one also can see that the width of the diffraction peaks gradually broaden with decreasing annealing temperature, while the intensity of the diffraction peaks increases with increasing annealing temperature. The calculated grain sizes (derived from Scherrer's formula) are about 3.4, 7.2, 15.4 and 53.5 nm for the VO₂ (M) NPs annealed at 300, 350, 400 and 450 °C, respectively (Table 1), which are all smaller than the calculated value (Fig. S2†). This indicates that the VO₂ (M) NPs are polycrystalline. HRTEM observations show that the defect concentration in the VO₂ (M) NPs depends on the annealing temperature, and the VO₂ (M) NPs obtained at 300 °C contain abundant lattice distortions and grain boundaries (Fig. S3a and b†), which are absent from the VO₂ (D) NPs before annealing. In most cases, these defects are the inevitable consequence of the intergrowth structure¹⁵ and serve as the origin of the relative poor crystallization of VO₂ (M), as shown in Fig. 1d. The lattice distortions disappear while a small quantity of the grain and twin boundaries survive as the annealing temperature increases to 400 °C (Fig. S3c and d†). Meanwhile, the crystallinity is improved (Fig. 1d), and the reduced defect concentration is considered to have great influence on the phase transformation behavior of VO₂ (M).

DSC analysis provided definitive evidence of the formation of VO₂ (M) due to the noticeable first-order structural transition of VO₂ (M \leftrightarrow R). Clear, sharp peaks attributed to the M \leftrightarrow R phase transition can be observed in the DSC curves (Fig. S4†). The peak temperatures are summarized in Table 1, from which one can see that, during the heating cycle, T_c can be depressed to as low as 37.4 °C from 78.6 °C when the annealing temperature is decreased from 450 to 300 °C. A similar steady decrease from 60.68 to 27.1 °C can be observed for cooling cycle. It is worth noting that T_c can be effectively tuned to near room temperature, while the thermal hysteresis can be simultaneously narrowed as shown in Table 1, which reflects the finite size effect of the VO₂ (M) NPs for T_c depression.^{16–18} The mechanism of the hysteresis broadening has been discussed by Lopez *et al.* in terms of a heterogeneous nucleation process,¹⁹ where the phase transition depends on the availability of a suitable nucleating defect in the sample space considered. A lower T_c and a larger thermal hysteresis will be obtained with decreasing NP size due to the reduced number of defects within the relevant volume.²⁰ However, in the present study, the hysteresis width decreases to 10.3 °C from 18.04 °C as the grain size decreases from 53.5 to 3.4 nm, indicating that the small grains possess a narrower hysteresis. This kind of discrepancy also has been observed by Xie *et al.*, and is mainly considered to be due to surface defects.²¹ We attribute this inconformity to an interfacial effect.^{22–24} As the internal interface (between the grain and twin boundaries) formed in a NP during the phase transition of VO₂ (D) \rightarrow VO₂ (R) can act as a nucleation site, this leads to a significant decrease in the hysteresis width. There is competition between the size effect and interfacial defects in determining the T_c and hysteresis width. At a lower annealing

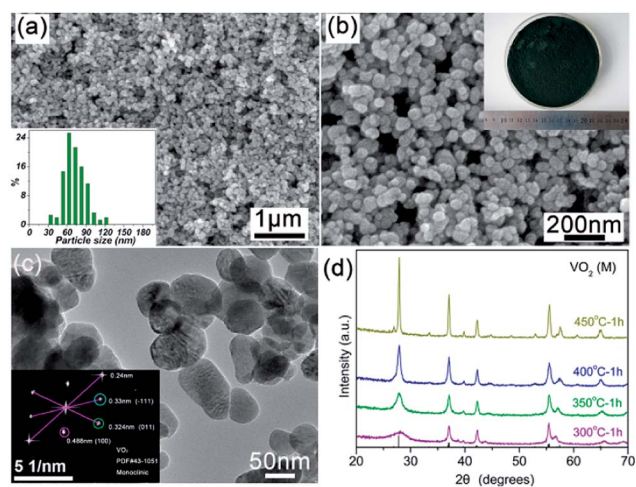


Fig. 1 (a) Low and (b) high magnification FESEM images of the VO₂ (M) NPs; the insets in (a) and (b) show the particle size distribution and a digital photograph of the large-scale NP production, respectively; (c) and (d) show the corresponding TEM image and XRD patterns of the VO₂ (M) NPs; the inset in (c) shows the corresponding SAED pattern.

Table 1 DSC results for the cooling and heating cycles of the VO₂ (M) NPs obtained at different annealing temperatures

$T_{\text{annealing}}$ (°C)	$T_{\text{c-heating}}$ (°C)	$T_{\text{c-cooling}}$ (°C)	ΔT (°C)	Grain size (nm)
300	37.37	27.11	10.26	3.4
350	58.83	45.81	13.02	7.2
400	72.59	56.56	16.03	15.4
450	78.62	60.58	18.04	53.5

temperature, interfacial defects play an essential role in triggering the phase transformation of VO₂ (M) leading to a depressed T_{c} and narrow hysteresis. With the increasing annealing temperature the defect concentration reduces gradually and the size effect dominates, resulting in a high T_{c} and a broad hysteresis.

It was found that the annealing time and vacuum also affect the phase transition of the VO₂ (M) NPs. So far as T_{c} is concerned, using a low annealing temperature over a long time duration is equal to using a high temperature over a short time (Fig. S5†). The T_{c} of VO₂ obtained by annealing at 300 °C for 3 h is close to that obtained at 350 °C for 1 h using the same vacuum conditions. The vacuum has no obvious influence on the size and crystal quality of the VO₂ (M) NPs (as shown by XRD analysis), however the T_{c} slightly increases as the vacuum is decreased due to the stoichiometry of the VO₂ (M) NPs, which is consistent with recent experiment results.^{8,25}

After mixing with PVP in alcohol [5 wt% PVP and 5 wt% VO₂ (M)], VO₂ (M) NP thin films were obtained on glass substrates by spin-coating the VO₂ (M) NPs annealed at 450 °C. The temperature-dependent transmittance of VO₂ (M) NP thin films with three different thicknesses are shown in Fig. 2 (the insets to the right show the corresponding photographs). For the thinnest film (curve 1), the infrared transmittance is about 89.5 and 53.8% before and after the M ↔ R phase transition, respectively, at a wavelength of 1.5 μm with the infrared modulation over 35%, which is high enough to be used as an intelligent

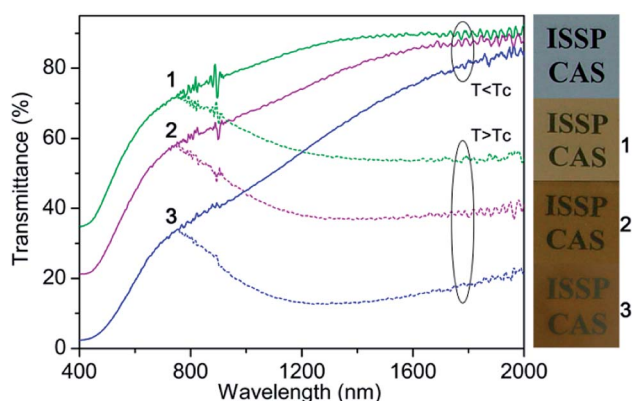


Fig. 2 Optical transmittance and the corresponding photographs (the topmost photo is a bare glass substrate) of the VO₂ (M) thin films with thicknesses of 463 (curve 1), 730 (curve 2) and 1175 (curve 3) nm prepared by spin-coating VO₂ (M) NP annealed at 450 °C on glass substrates.

window material. This film also shows favourable visible light transmittance (over 70% at 700 nm and 65% at 600 nm), which is higher than that of SiO₂/VO₂ composite foils,²⁶ and as high as the recently reported porous VO₂ (M) films.²⁷ As film thickness increases, the infrared modulation increases and the visible light transmittance decreases, demonstrating that a high infrared modulation can be achieved at the cost of visible transmittance. In order to balance the visible transmittance and infrared modulation ability, the optimal thickness (curve 1) should be used, which can achieve excellent thermochromic performance. Theoretical calculations by Granqvist *et al.* indicated that VO₂ nanoparticles dispersed in a dielectric matrix offer a number of specific advantages over VO₂-based continuous films for simultaneously enhancing luminous transmittance and solar energy modulation.⁹ The high thermochromic performance of the VO₂ (M) NPs dispersed in the PVP host in the present study provides further evidence to support this prediction. It was found that the VO₂ (M) NP thin films derived from NPs annealed at 400, 350 and 300 °C also exhibited good thermochromic performance with infrared modulations of over 25% and relative low T_{c} values (see Fig. S6† and Table 1).

An external electric field also can drive the insulator–metal transition of VO₂ (M) at room temperature. Fig. 3a shows the I – V curve of the VO₂ (M) NPs annealed at 300 °C (a TEM image of the tungsten tip and the corresponding NPs during the *in situ* electrical test can be found in Fig. S7†). One can see that the current gradually increases as the voltage increases from 0 to 0.85 V, and then abruptly increases at 0.81 V. The roughness of the plot is due to the abundant defects in the VO₂ (M) NPs. The inset in Fig. 3a demonstrates that the phase transition can be triggered within 95.6 ms. Fig. 3b shows I – V curves of VO₂ (M) NPs annealed at 450 °C (each curve is obtained from different nanoparticles in the same sample), a sharp jump in the current can be clearly observed at a threshold voltage of about 1 V. Note that the bias voltage required to drive the phase transition of the VO₂ (M) NPs depends on the morphology, dimensions and temperature. The inset in Fig. 3b also shows the ultra-fast phase transformation characteristics of VO₂ (M) NPs. The above results clearly demonstrate that the phase switching of the VO₂ (M) NPs can be activated with a relatively low voltage at room temperature, which may provide a new pathway to construct VO₂-based films with electrically induced thermochromic properties that achieve energy-saving in building.

In summary, an effective strategy has been developed to fabricate highly crystalline VO₂ (M) NPs on a large scale by mildly annealing a hydrothermal product. The phase transition temperature of the VO₂ (M) NPs can be regulated *via* a size effect and interfacial defects rather than the traditional doping methods. The VO₂ (M) NP thin film shows an excellent thermochromic performance with high visible transmittance (70%) and infrared modulation (>35%). The low threshold voltage (*ca.* 1 V) is adequate to trigger the phase transition of the VO₂ (M) NPs at room temperature. Our results open a new avenue for constructing VO₂-based thermochromic films.

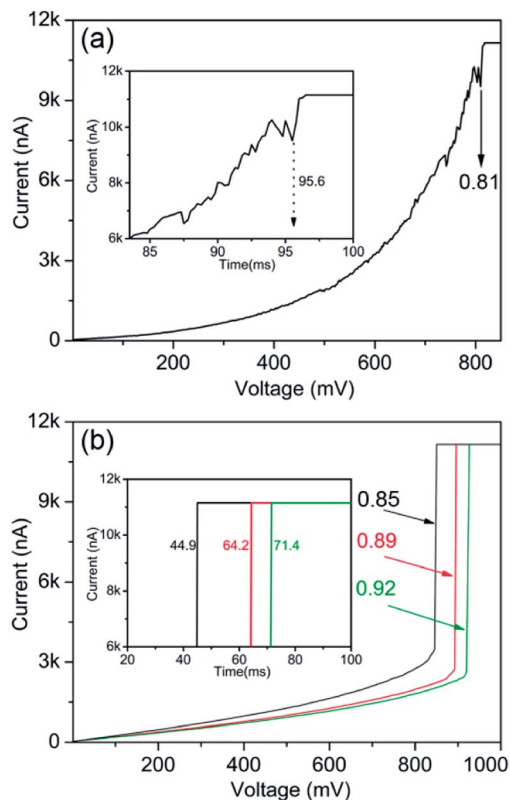


Fig. 3 I - V curves of VO_2 (M) NPs obtained at (a) $300\text{ }^\circ\text{C}$ and (b) $450\text{ }^\circ\text{C}$. The insets are the corresponding detail current enhancement that immediate proximity to the saturation current with time.

Acknowledgements

The authors acknowledge the National Natural Science Foundation of China (Grant 51372250) and the National Basic Research Program of China (Grant 2009CB939903). X. W. acknowledges financial support from Chinese postdoctoral funding (no. 2012M520053). L. S. acknowledges Jiangsu Province Funds for Distinguished Young Scientists (no. BK2012024).

References

- 1 J. H. Park, J. M. Coy, T. S. Kasirga, C. Huang, Z. Fei, S. Hunter and D. H. Cobden, *Nature*, 2013, **500**, 431–434.
- 2 Y. Gao, H. Luo, Z. Zhang, L. Kang, Z. Chen, J. Du, M. Kanehira and C. Cao, *Nano Energy*, 2012, **1**, 221–246.
- 3 T. D. Manning, I. P. Parkin, M. E. Pemble, D. Sheel and D. Vernardou, *Chem. Mater.*, 2004, **16**, 744–749.

- 4 S. Babulanam, T. Eriksson, G. Niklasson and C. Granqvist, *Sol. Energy Mater. Sol. Cells*, 1987, **16**, 347–363.
- 5 Z. Lu, C. Li and Y. Yin, *J. Mater. Chem.*, 2011, **21**, 14776–14782.
- 6 J. B. Goodenough, *J. Solid State Chem.*, 1971, **3**, 490–500.
- 7 J. Zhang, H. He, Y. Xie and B. Pan, *J. Chem. Phys.*, 2013, **138**, 114705.
- 8 J. Jeong, N. Aetukuri, T. Graf, T. D. Schladt, M. G. Samant and S. S. P. Parkin, *Science*, 2013, **339**, 1402–1405.
- 9 S.-Y. Li, G. A. Niklasson and C. G. Granqvist, *J. Appl. Phys.*, 2010, **108**, 063525.
- 10 J. M. Booth and P. S. Casey, *ACS Appl. Mater. Interfaces*, 2009, **1**, 1899–1905.
- 11 Z. Xu, D. Golberg and Y. Bando, *Nano Lett.*, 2009, **9**, 2251–2254.
- 12 Z. L. Wang and J. Song, *Science*, 2006, **312**, 242–246.
- 13 L. Liu, F. Cao, T. Yao, Y. Xu, M. Zhou, B. Qu, B. Pan, C. Wu, S. Wei and Y. Xie, *New J. Chem.*, 2012, **36**, 619–625.
- 14 A. Pan, H. B. Wu, L. Yu and X. W. D. Lou, *Angew. Chem., Int. Ed.*, 2013, **125**, 2282–2286.
- 15 J. Xie, C. Wu, S. Hu, J. Dai, N. Zhang, J. Feng, J. Yang and Y. Xie, *Phys. Chem. Chem. Phys.*, 2012, **14**, 4810–4816.
- 16 L. Whittaker, C. Jaye, Z. G. Fu, D. A. Fischer and S. Banerjee, *J. Am. Chem. Soc.*, 2009, **131**, 8884–8894.
- 17 S. Chen, H. Ma, J. Dai and X. Yi, *Appl. Phys. Lett.*, 2007, **90**, 101117.
- 18 M. Nazari, Y. Zhao, V. Hallum, A. A. Bernussi, Z. Y. Fan and M. Holtz, *Appl. Phys. Lett.*, 2013, **103**, 043108.
- 19 R. Lopez, T. E. Haynes, L. A. Boatner, L. C. Feldman and R. F. Haglund, *Phys. Rev. B: Condens. Matter Mater. Phys.*, 2002, **65**, 224113.
- 20 R. Lopez, L. C. Feldman and R. F. Haglund, *Phys. Rev. Lett.*, 2004, **93**, 177403.
- 21 Y. Sun, S. Jiang, W. Bi, R. Long, X. Tan, C. Wu, S. Wei and Y. Xie, *Nanoscale*, 2011, **3**, 4394–4401.
- 22 K. Appavoo, D. Y. Lei, Y. Sonnefraud, B. Wang, S. T. Pantelides, S. A. Maier and R. F. Haglund, *Nano Lett.*, 2012, **12**, 780–786.
- 23 E. U. Donev, R. Lopez, L. C. Feldman and R. F. Haglund Jr, *Nano Lett.*, 2009, **9**, 702–706.
- 24 J. Du, Y. Gao, H. Luo, L. Kang, Z. Zhang, Z. Chen and C. Cao, *Sol. Energy Mater. Sol. Cells*, 2011, **95**, 469–475.
- 25 S. Zhang, I. S. Kim and L. J. Lauhon, *Nano Lett.*, 2011, **11**, 1443–1447.
- 26 Y. Gao, S. Wang, H. Luo, L. Dai, C. Cao, Y. Liu, Z. Chen and M. Kanehira, *Energy Environ. Sci.*, 2012, **5**, 6104–6110.
- 27 M. Zhou, J. Bao, M. Tao, R. Zhu, Y. Lin, X. Zhang and Y. Xie, *Chem. Commun.*, 2013, **49**, 6021–6023.